1992MNRAS.255..713T

Mon. Not. R. astr. Soc. (1992) **255**, 713–728

The starburst model for active galactic nuclei: the broad-line region as supernova remnants evolving in a high-density medium

Roberto Terlevich,[1] Guillermo Tenorio-Tagle,[2] Jose Franco[3] and Jorge Melnick[4]

[1]*Royal Greenwich Observatory, Madingley Road, Cambridge, CB3 0EZ*
[2]*Instituto de Astrofísica de Canarias, 38200 La Laguna, Tenerife, Spain*
[3]*Instituto de Astronomía UNAM, Apartado Postal 70-264, 04510 México D. F., México*
[4]*European Southern Observatory, Casilla 19001, Santiago, Chile*

Accepted 1991 November 20. Received 1991 November 20; in original form 1991 July 23

SUMMARY

It is shown that the broad permitted and semipermitted emission lines of the broad-line region (BLR) of radio-quiet active galactic nuclei (AGN) can be generated by strongly radiative (rapidly cooling) supernova remnants expected to occur in the central regions of early-type galaxies undergoing a starburst. Supernova remnants interacting with a circumstellar medium with a density of about $n \sim 10^7$ cm^{-3} become strongly radiative while still expanding at several thousand km s^{-1}, and miss the adiabatic Sedov track. Radiative cooling becomes important well before the thermalization of the ejecta is completed, and the shocked matter undergoes a fast condensation behind both the outgoing forward shock and the reverse shock. Two concentric, high-density, and fast-moving thin shells are then formed. Both cool dense shells, as well as the expanding ejecta, the unshocked circumstellar material and a section of the interstellar gas, are irradiated and ionized by the photon field produced by the radiative shocks.

Our model, in which the only free parameter is the density of the circumstellar medium, combines analytic and numerical hydrodynamic simulations, together with static photoionization computations, to reproduce most of the basic properties of the BLR in low-luminosity AGN.

1 INTRODUCTION

One of the most puzzling properties of AGN is that they emit an enormous amount of energy over a large range in wavelength from an apparently very small volume. The emitting volumes have been constrained by the observed variability time-scale and, if the source of energy is a single object, the typical sizes inferred are of the order of 10^{-2} pc.

The nature of the energy source of AGN is perhaps the most fundamental aspect of their study. Most researchers agree that the energy source in AGN is primarily gravitational and involves large concentrations of matter such as extremely dense stellar clusters, supermassive stars, or massive black holes. However, the idea that both dense stellar clusters and supermassive stars may end their evolution as massive black holes (Rees 1977, 1978, 1984) has shifted the aim of theoretical and observational work towards the study of the properties of these latter objects and their environment. Thus, a 'canonical' model has evolved whereby AGN are powered by accretion discs circling massive black holes. This model postulates also the existence of small high-density clouds very close to the nucleus where only broad permitted lines are formed – the BLR – and a more extended system of low-density filaments where narrow forbidden and permitted lines are formed – the NLR. The line widths of the BLR (up to 10 000 km s^{-1} FWHM) are assumed to reflect the motions of the ensemble of cold ($T_{\rm eff} \sim 10^4$ K), dense ($n \sim 10^{10}$ cm^{-3}) clouds moving in the gravitational field of the massive central object. The ionizing spectrum is assumed to follow a power law of the form $f_\nu \propto \nu^{-1.0}$ up to a few hundred keV. Other typical parameters of these clouds, also derived from the photoionization models (e.g. Collin-Souffrin 1990), are the ionization parameter $U \sim 2 \times 10^{-3}$ and column density $\sigma \sim 10^{23}$ cm^{-2}. In total, the BLR contains from about 1 $M_\odot$ for Seyfert 1 nuclei, to about 100 $M_\odot$ in luminous QSOs, in clouds which fill only a small fraction of the volume. While this model is very successful in accounting for many of the observed properties of the BLR of AGN, it is also unsatisfactory in that it requires a large number of arbitrary parameters which cannot be predicted from theory and are freely adjusted to match the observations.

An alternative to account for the activity of AGN is the *starburst* or *AGN without Black Holes* model. This model postulates that star-formation activity can power AGN with-

Downloaded from https://academic.oup.com/mnras/article/255/4/713/1310600 by guest on 20 August 2022

© Royal Astronomical Society • Provided by the NASA Astrophysics Data System

1992MNRAS.255..713T

out the need for massive black holes (Terlevich, Melnick & Moles 1987; Terlevich 1989). It was first proposed to account for the properties of radio galaxies and quasars (Shklovskii 1960; Field 1964; McCrea 1976) but was abandoned because it failed to explain satisfactorily the variability of luminous quasars, their radio emission and compact radio cores, and the presence of broad permitted and narrow forbidden emission lines and their intensity ratios. In the starburst model, nuclear activity is the *direct* consequence of the evolution of a massive young cluster of coeval stars in the high metal abundance environment of the nuclear region of early-type galaxies (Pagel & Edmunds 1981; Díaz, Pagel & Wilson 1985). In this scenario, nuclear activity is the natural consequence of the *final* stages of galaxy formation, i.e. when the core of the spheroidal component of an otherwise normal galaxy forms in a short time most of the old stars we see today (Terlevich 1992).

The phenomenology of narrow-line AGN (Seyfert 2 and LINERS) and its relation to nuclear starbursts has been analysed by Terlevich & Melnick (1985, hereafter TM85) who further predicted an evolutionary sequence which follows the evolution of a coeval nuclear cluster. For luminous objects, the nuclear emission-line regions evolve from normal H II regions to type 2 Seyferts and later to LINERS with transitions after about 3 and 5 Myr, respectively. The subsequent evolution of these young clusters into the supernova phase and the development of the BLR have been described by Terlevich *et al.* (1987), Terlevich & Melnick (1987, 1988) and Terlevich (1989, 1990a, b). In these latter models, a substantial part of the bolometric luminosity emitted during the quasar phase is due to young stars, while the observed broad permitted emission lines and their variability are due to supernova (SN) and supernova remnant (SNR) activity (Terlevich & Melnick 1987, 1988; Terlevich 1989; Filippenko 1989; Terlevich 1990b). Low-luminosity highly variable Seyfert type 1 nuclei could host only 1 SNR at any one time, whereas the less variable and more luminous quasar may typically contain some 100 coexisting SNR in different stages of evolution (Terlevich 1990b).

Although the spectra of SN and galactic remnants do not resemble the spectra of AGN, recent observations show that at least some luminous SN exploding in H II regions have a striking resemblance to broad-line Seyfert galaxies (Filippenko 1989), and, conversely, that the flares of some Seyfert galaxies have the luminosity, life-time and spectral signatures of type II SN (Terlevich & Melnick 1988). The fundamental difference between 'Seyfert-like' and normal type II SN can be understood if the former are associated with shocks expanding into regions of high interstellar or circumstellar gas densities. Theoretical computations of the evolution of SNR in dense molecular clouds show that, after sweeping up a small amount of gas and when their sizes are only few light-weeks across, these remnants become strongly radiative and deposit most of their (kinetic) energy in very short time-scales, thus reaching very high luminosities. Because of the large shock velocities, most of the energy is radiated in the extreme UV and X-ray region of the spectrum (e.g. Shull 1980; Wheeler, Mazurek & Sivaramakrishnan 1980). In our scenario, these SNR are the BLR.

This paper describes a study of the evolution of SNR in a high-density medium by means of analytical and numerical hydrodynamic and photoionization models, which show that these SNRs have properties (luminosity, density, size, kinematics, emission line ratios, variability time-scales and energy, etc.) which are essentially identical to those considered typical of the BLR. We discuss a single remnant because, for normal young stellar clusters with the luminosity of luminous AGN, these remnants are isolated systems that do not interact with each other. This happens for even the most dense of the massive stellar systems. Terlevich (1992) suggested that the 'isothermal' cores of elliptical galaxies, forming at the end of the collapse of the spheroid at a redshift of about 2 to 3, could be the QSOs. The core of a typical (L^*) elliptical has a velocity dispersion of about 200 km s^{-1}, a radius of about 200 pc, a total mass of about $2 \times 10^{10}\ M_\odot$, and, if it is formed in a crossing time (about 1.5 Myr), an absolute blue luminosity of about $M_b = -25$, similar to the luminosity of a typical (L^*) QSO. The supernova rate will be about 12 per year and the remnants will be distributed across the core region with typical distances between remnants of about 100 pc. As the final radius of these remnants is well below 1 pc no superposition of remnants is expected in these young cores.

The paper is organized as follows: Section 2 presents hydrodynamical models which follow the evolution of SNRs in very high-density media. Section 3 presents photoionized models of the various components of the SNRs and Section 4 compares the predicted emerging spectra and other computed parameters with the observations of the BLR of Seyfert galaxies and QSOs.

2 SUPERNOVA REMNANTS IN HIGH-DENSITY MEDIA

2.1 Early analytical models of SNR evolution in high densities

Type II SN explode inside the gas structures created by the previous activity of the progenitors (i.e. wind-driven bubbles and H II regions). Observational evidence for these pre-existing extended circumstellar shells exists both in our Galaxy and in external galaxies (see review by Franco *et al.* 1991).

The interaction of SN ejecta with circumstellar material can have a variety of important effects (Chevalier & Liang 1989; Tenorio-Tagle *et al.* 1990, 1991; Franco *et al.* 1991). These depend on the radial density distribution created by the pre-SN activity, which in turn is also dependent on the ambient interstellar conditions, provided that the central regions of galaxies have a high interstellar medium density ($n \sim 10^{3-4}$ cm^{-3}) and any embedded gaseous structure is subjected to large system pressures (i.e. much larger than those found in the solar circle). In particular, as the average ambient medium is highly pressurized, the resulting sizes of wind-driven structures are reduced whereas their densities are increased. As a result, the SN explosions will occur inside a dense shell. Also, a few solar masses of material at a distance of $\sim 10^{16}$ cm, such as that ejected during the neon or oxygen flashes at the late stages of stellar evolution (Woosley, Weaver & Taam 1980) or in a cool and slow wind during the red supergiant phase (Dupree 1986), can radiate a large fraction of the kinetic energy of the SN in a very short time, thus producing a luminous and spectacular event.

The initial interaction of the SN ejecta with the ambient medium causes a shocked region of hot gas enclosed by two shock waves: on the outside the outgoing shock, and on the

Downloaded from https://academic.oup.com/mnras/article/255/4/713/1310600 by guest on 20 August 2022

© Royal Astronomical Society • Provided by the NASA Astrophysics Data System

1992MNRAS.255..713T

inside the inward-looking reverse shock. The outward shock ($V \sim 10^4$ km s^{-1}) encounters dense circumstellar material and raises its temperature to $\sim 10^9$ K. The reverse shock, which is substantially slower ($V \sim 10^3$ km s^{-1}), thermalizes the SN ejecta to temperatures of about $\sim 10^7$ K. Early analytical and numerial computations of the evolution of SNRs in a dense medium (Chevalier 1974; Shull 1980; Wheeler *et al.* 1980) showed a much faster evolution relative to the 'standard' solution in a medium of density $n_0 = 1$ cm^{-3}. All evolutionary phases (free expansion, thermalization of the ejecta, the quasi-adiabatic Sedov phase, the radiative and the pressure-modified snow-plough phases), which have been thoroughly studied for the standard case, are substantially speeded up.

The onset of the radiative phase behind the leading shock (under the assumption of free–free cooling only) causes the formation of a dense outer shell and, for a supernova remnant injecting 10^{51} erg in a medium of constant density $n_7 = n_0/10^7$ cm^{-3} (Shull 1980; Wheeler *et al.* 1980), begins at time t_{sg} given by

$$t_{sg} = 230\, E_{51}^{1/8} n_7^{-3/4} \text{ d} \tag{1}$$

where E_{51} is the energy deposited by the SN in units of 10^{51} erg. At this stage, the velocity (V), radius (R), temperature (T), and luminosity (L) of the shock are

$$V_{shock} = 4600\, E_{51}^{1/8} n_7^{1/4} \left(\frac{t}{t_{sg}}\right)^{-5/7} \text{km s}^{-1}, \tag{2}$$

$$R_{shock} = 0.01\, E_{51}^{1/4} n_7^{-1/2} \left(\frac{t}{t_{sg}}\right)^{2/7} \text{pc}, \tag{3}$$

$$T_{shock} = 3.0 \times 10^8\, E_{51}^{1/4} n_7^{1/2} \left(\frac{t}{t_{sg}}\right)^{-10/7} \text{K}, \tag{4}$$

$$L_{shock} = 2 \times 10^{43}\, E_{51}^{7/8} n_7^{3/4} \left(\frac{t}{t_{sg}}\right)^{-11/7} \text{erg s}^{-1}. \tag{5}$$

The shocked circumstellar medium in the cavity behind the outward shock will produce a luminosity

$$L_{cavity} = 2 \times 10^{42}\, E_{51}^{7/8} n_7^{3/4} \left(\frac{t}{t_{sg}}\right)^{-8/7} \text{erg s}^{-1}. \tag{6}$$

Assuming an even pressure behind the shock, these equations can be combined to obtain indicative values of density (n), ionization parameter (U), mass (M), and column density (σ) of the outer shell of swept-up matter,

$$n_{shell} = 1.2 \times 10^{12}\, E_{51}^{1/4} n_7^{3/2} \left(\frac{t}{t_{sg}}\right)^{-10/7} \text{cm}^{-3}, \tag{7}$$

$$U_{shell} = 2.0 \times 10^{-4}\, E_{51}^{1/8} n_7^{-1/4} \left(\frac{t}{t_{sg}}\right)^{-5/7}, \tag{8}$$

$$M_{shell} = 1.1\, E_{51}^{3/4} n_7^{-1/2} \left(\frac{t}{t_{sg}}\right)^{6/7} M_\odot, \tag{9}$$

$$\sigma_{shell} = 1.1 \times 10^{23}\, E_{51}^{1/4} n_7^{1/2} \left(\frac{t}{t_{sg}}\right)^{2/7} \text{cm}^{-2}, \tag{10}$$

Notice that for densities close to $n_7 \sim 1$, and $t > t_{sg}$, equations (2) to (5) give values very close to those typical of low-luminosity AGN, while equations (7) to (10) give values that are strikingly similar to those that characterize the region that emits the Low Ionization Line system of the BLR (see Collin-Souffrin & Lasota 1988, and Section 4.1).

The properties of the reverse shock can also be inferred for a given set of initial conditions. In the case of an explosion within a cavity generated by a previous wind, the reverse shock is weaker and therefore the temperature of the shocked ejecta is lower than that acquired behind the outward shock (Band & Liang 1989; Tenorio-Tagle *et al.* 1991). Because of its lower temperature, most of the luminosity of the reverse shock will be emitted in the soft X-ray to UV part of the spectrum and the associated post-shock shell will have lower density and much higher ionization parameter than the outer shell. We identify the reverse shock and the reverse shock shell with the region of the BLR responsible for the High Ionization Line system.

2.2 The limitations of the analytical models

These approximate formulae, which are used here only as a guideline, assume that the ejecta have been already fully thermalized. However, for large values of n_0 (say for $n_0 \geq 10^5$ cm^{-3}), strong radiative losses due to free–free emission occur before thermalization is completed (see equation 1). This happens even if the forward shock velocity is assumed to remain constant, say at 10^4 km s^{-1} (or $V_9 = 1$, which provides a lower limit), since to sweep up 40 to 50 times the ejected mass (when $M_{ej} \sim 1$–$5\ M_\odot$; e.g. Gull 1973), or say a total average of 100 $M_\odot$ ($M_{100} \sim 1$), requires a thermalization time $t_{th} = 4.8$ yr $V_9^{-1} M_{100}^{1/3} n_7^{-1/3}$, much larger than t_{sg}. In fact, at large densities the cooling radiates the thermal energy at the same rate as thermalization proceeds. Thus the Sedov phase is totally inhibited and there is no self-consistent analytic treatment for the evolution of such remnants (but see Fig. 6). It is therefore necessary to follow the detailed time evolution of the gas flow. In particular, special care should be given to the post-shock structure which is sensitive to the details of the ambient density distribution and to the temperature dependence of the radiative cooling function. For an optically thin plasma, the cooling time, t_c, is proportional to the inverse of the gas density and the evolution proceeds faster at higher ambient densities. The temperature dependence of the cooling function, on the other hand, is different for different temperature ranges. Adiabatic shocks are stable but cooling instabilities can develop over a wide range of radiative shock conditions (e.g. Avedisova 1974; Falle 1975, 1981; McCray, Stein & Kafatos 1975; Chevalier & Imamura 1982; Imamura 1985; Bertschinger 1986).

The details of the transition from a nearly adiabatic to a strongly radiative shock depend on the ability of the gas to readjust to the cooling rate (see Franco *et al.* in preparation). Pressure gradients tend to be smoothed out in a sound crossing time, t_d, and the ratio t_c/t_d provides an estimate of the conditions prevailing in the cooling gas. For $t_c/t_d > 1$, at moderate cooling rates, the gas elements are continuously compressed as their temperature drops and the cooling process operates quasi-isobarically at the pressure attained by the gas immediately behind the shock. For $t_c/t_d < 1$, however, the cooling rate dominates over any pressure readjustment and

Downloaded from https://academic.oup.com/mnras/article/255/4/713/1310600 by guest on 20 August 2022

© Royal Astronomical Society • Provided by the NASA Astrophysics Data System

1992MNRAS.255..713T

the process becomes quasi-isochoric at the post-shocked density of the cooling gas elements. A large pressure imbalance then develops in the flow, and new additional shocks are generated which end up compressing the cooled gas. This process, termed 'catastrophic cooling' (Falle 1975, 1981), appears during thin shell formation and the instabilities continue to operate during the rest of the radiative shock evolution (e.g. Chevalier & Imamura 1982; Bertschinger 1986; Cioffi, McKee & Bertschinger 1988; Tenorio-Tagle *et al.* 1990).

In the present computations of SN evolving in ambient densities of the order of $n_0 \sim 10^7$ cm^{-3}, the cooling time- and length-scales for the post-shock temperatures are very small:

$$t_c \simeq \frac{3kT_s}{8n_0\Lambda} \simeq 0.2\,\frac{v_8^2}{n_7\Lambda_{23}}\ \text{yr}, \tag{11}$$

$$r_c \simeq \frac{1}{4}\,t_c v_s \simeq 1.8\times10^{14}\,\frac{v_8^3}{n_7\Lambda_{23}}\ \text{cm}, \tag{12}$$

where $v_8 = v/10^8$ km s^{-1} and $\Lambda_{23} = \Lambda/10^{-23}$ erg cm^3 s^{-1}. Thus radiative losses become important at very early times when the shock velocities and temperatures are $v_s > 10^3$ km s^{-1} and $T_s > 10^7$ K, well before the ejecta are even thermalized. These features imply, as in the colliding cloud model by Daltabuit *et al.* (1978), that a large flux of ionizing photons will emerge from the shocked gas. The wide range of gas temperatures in the cooling region results in a 'power-law'-like spectrum at UV and X-ray frequencies. These details, the specific temperature structure of the cooling region and the resulting photon spectrum, cannot be resolved with the numerical simulations presented below, and have been approximated with the analytical solutions given in Section 2.4.

2.3 Numerical hydrodynamic models

Numerical simulations of SN explosions in a constant density medium of $n_0 = 1$ cm^{-3} (the standard case) have been performed by several authors with a variety of computational codes and initial conditions (see Tenorio-Tagle *et al.* 1990 and references therein). From these we have learned about the various complications that have to be resolved to calculate a 'realistic' evolution. Calculations in a higher density medium lead to further complications, mainly due to the required higher spatial resolution. However, given the expected speeded-up evolution and thus the smaller final radius, attempts can be made to calculate with reasonable accuracy the evolution at higher densities with the computational facilities now available.

We present here the evolution of a SNR caused by the release of $E_0 = 10^{51}$ erg into a constant density medium of $n_0 = 10^7$ cm^{-3}. The density and velocity distributions of the ejecta were scaled from the explosion models given by Woosley, Pinto & Ensman (1988). Different simulations with ambient densities ranging from 1 to 10^5 cm^{-3} were performed to corroborate the validity of the numerics. Models were obtained in one and two dimensions with the hydrodynamical codes described by Tenorio-Tagle *et al.* (1990) and Różyczka (1985), respectively. The 1D approach is based on a standard explicit time difference method to solve the hydrodynamical equations written in a Lagrangian formulation under the assumption of spherical symmetry. The 2D code is an axisymmetric Eulerian second-order advection scheme, also tested under a wide variety of conditions. Both codes account for radiative cooling as given by Raymond, Cox & Smith (1976) for solar abundance ($Z = Z_\odot$), and compute the degree of ionization under the assumption of collisional equilibrium. A total of 1800 grid points, initially equally spaced in radius ($\Delta r = 3\times10^{13}$ cm), were used to represent the unperturbed high-density background gas. This was placed in front of ejecta from a SN, assumed to have grown homologously to a distance of 1×10^{16} cm, while preserving a density and velocity structure as calculated by Woosley *et al.* (1988). For the 2D calculation, a 400×400 equally spaced grid was set to attain a resolution $\Delta r = \Delta z = 2.2\times10^{14}$ cm. In both cases the total energy deposited by the explosion is 10^{51} erg, with an ejected mass of 2.5 $M_\odot$ and a momentum of 2.44×10^{42} g cm s^{-1}. The velocity of the ejected matter, scaled proportional to radius, fell in the range 1000–16 000 km s^{-1}.

Fig. 1 shows the run of kinetic and thermal energy of the remnant as a function of time. Given the large densities and thus the strong radiative cooling, the combination of values of thermal ($E_{th} \sim 0.7\ E_0$) and kinetic ($E_k \sim 0.3\ E_0$) energies which characterizes the Sedov solution is never achieved. Instead, the thermal energy content is radiated away within the first five years of evolution, before the thermalization of the ejecta is completed. Calculations also show how both energies continuously drop after strong cooling occurs, and values of E_{th} much smaller than $0.1\ E_0$ are soon achieved. Such low values of E_{th} occur in the standard case some 10^6 yr after the explosion. The present solution thus indicates a speeded-up evolution and, at $t = 10$ yr, most of the injected energy has been radiated away. The remaining kinetic energy, a major fraction of which is stored in the outer shell of the remnant, is also rapidly decaying. Clearly, from the similar rate of change of both E_{th} and E_k towards the end of the calculated evolution, this energy is radiated as soon as it is thermalized behind the shock waves.

Strong radiative cooling starts at about one year after the explosion. Such an event inhibits the storage of thermal energy and produces the steady enhancement of the total, X-ray and Hα luminosities shown in Fig. 2. The maximum luminosity is reached 2.5 years after blast, and then the total X-ray and bolometric luminosities rapidly decay.

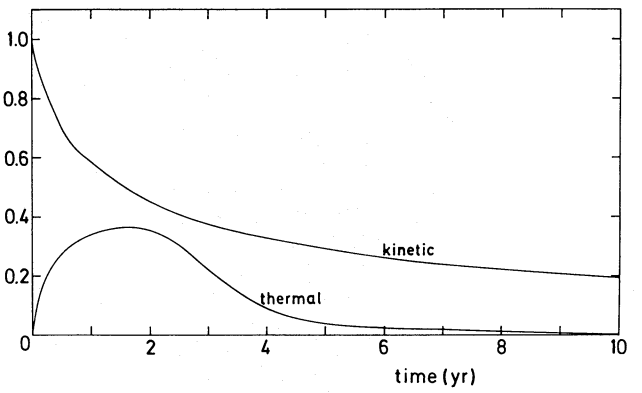

Figure 1. The evolution of remnants in a high-density environment. Total thermal and kinetic energies, in units of 10^{51} erg, as a function of time (in years).

Downloaded from https://academic.oup.com/mnras/article/255/4/713/1310600 by guest on 20 August 2022

© Royal Astronomical Society • Provided by the NASA Astrophysics Data System

1992MNRAS.255..713T

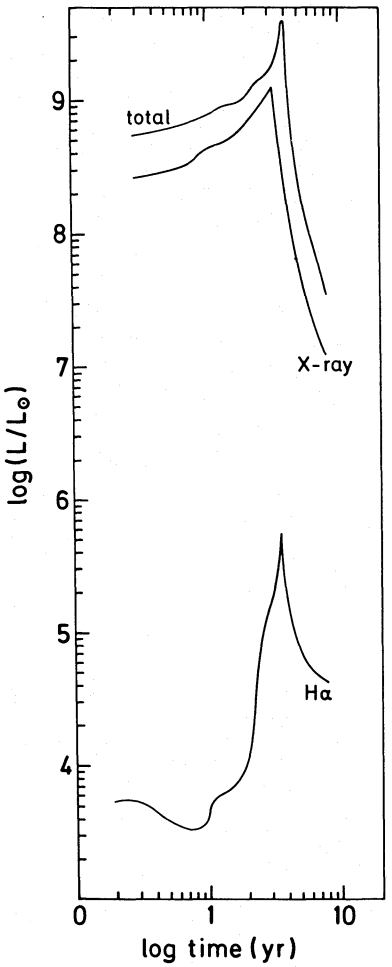

Figure 2. The evolution of remnants in a high-density environment. Total radiated luminosity and the integrated X-ray and Hα luminosities, as a function of time.

Fig. 3 shows the flow variables at different evolutionary times. Fig. 3(a) displays the flow after $t_{sn} = 0.53$ yr. The positions of both shocks (the forward shock and the reverse shock) are clearly indicated by the sudden changes in density and in all other plotted variables, while the contact discontinuity that separates shocked ejected matter from shocked interstellar gas appears as a spike in the density and temperature plots. This feature remains apparent until the end of the calculated evolution. At this early evolutionary time, the largest values of density and velocity are still determined by the initial condition of the unshocked ejecta, while the largest pressures and temperatures are found between the shocks. Also now, from the change in velocity across the shocks ($\Delta v \sim 5000$ km s^{-1}) and thus the post-shocked temperatures ($T \gg 10^8$ K), the two shocks have comparable strengths. Fig. 3(b) displays the same flow variables at a time soon after catastrophic cooling has occurred. This, given the large change in temperature, results in an enhancement of almost five orders of magnitude in the density of the interstellar shocked gas at the edge of the remnant. The condensed matter has cooled to the minimum allowed temperature of 8000 K, while it continues to move at more than 10^3 km s^{-1}.

Condensation is done via several secondary shocks. These shocks, however, being also in the rapid cooling regime, are unable to transmit, restore and keep up a pressure in the cooling zone similar to that of the hot cavity. Consequently, the leading forward shock undergoes rapid velocity and luminosity changes. Details of the thin shell formation behind the forward shock are shown in Fig. 4.

The effects of strong radiative cooling in the swept-up matter induce a sudden drop in gas pressure, and this leads to a rapid and noticeable deceleration of the forward shock. The process is followed by the condensation of most of the swept-up mass (about 90 per cent) which is located in the outer 10 per cent of the remnant radius (R_{snr}). This is pushed and condensed into a very thin shell (about 1 per cent R_{snr}) at the edge of the remnant, by several secondary shocks which eventually collide with the forward shock and increase its velocity (see Fig. 4). New matter entering the forward shock will then have to wait a cooling time to lose its pressure through radiation. Such an event will again lead to the deceleration of the leading forward shock, but the wall of condensed matter (the thin shell) will eventually sweep through the cooling region providing the shock wave with a larger speed. The process repeats itself several times with a period defined by the cooling time (t_c). Similarly, radiation behind the reverse shock accompanied by a sudden loss of pressure causes the outward displacement of the reverse shock. This leads to a smaller relative velocity between the shock and ejected matter, which promotes the weakening of the reverse shock and delays full thermalization even further. Also, as the separation of the two shells of swept-up matter becomes smaller, the reverse shock remains weaker compared to the outer one, while the freely expanding ejecta become rarer and cooler as they fill the remnant interior.

Similar results were also obtained in the 2D calculation. Fig. 5 is a mosaic of isodensity contour plots obtained at different evolutionary times. These show the development of the thin shell at the edge of the remnant as well as the collapse of the shocked ejecta behind the reverse shock. This calculation which also allows for the development of cooling instabilities clearly shows the steady approach of the two shells of cool matter, promoted by the weakening and withdrawal of the reverse shock while the unshocked ejecta fills the remnant interior. Other 2D calculations with a different initial condition, namely 10^{51} erg deposited as thermal energy within a small box centred at the grid origin, lead also to the same evolutionary features described above. Therefore the numerical solutions, despite different resolution and initial conditions, all show a small ($R_{snr} \sim$ a few times 10^{16} cm) rapidly radiating remnant, with two massive and geometrically thin concentric shells moving at large speeds and bounded by radiative shock waves. A small fraction of the swept-up mass lies between the two shocks and remains at very high temperatures (about 10^8 K). On the other hand, in the central regions of the remnant, the ejected matter continues to expand homologously, and thus represents a density and velocity distribution which reflects the initial condition, until it is thermalized at the reverse shock. This central region together with a section of the still unperturbed background gas and the two thin, cool shells, are clearly subjected to the ionizing radiation provided by the radiative shocks and the hot interior gas. As can be seen from Fig. 5, the 2D modelling displays a rich variety of structures.

Downloaded from https://academic.oup.com/mnras/article/255/4/713/1310600 by guest on 20 August 2022

© Royal Astronomical Society • Provided by the NASA Astrophysics Data System

1992MNRAS.255..713T

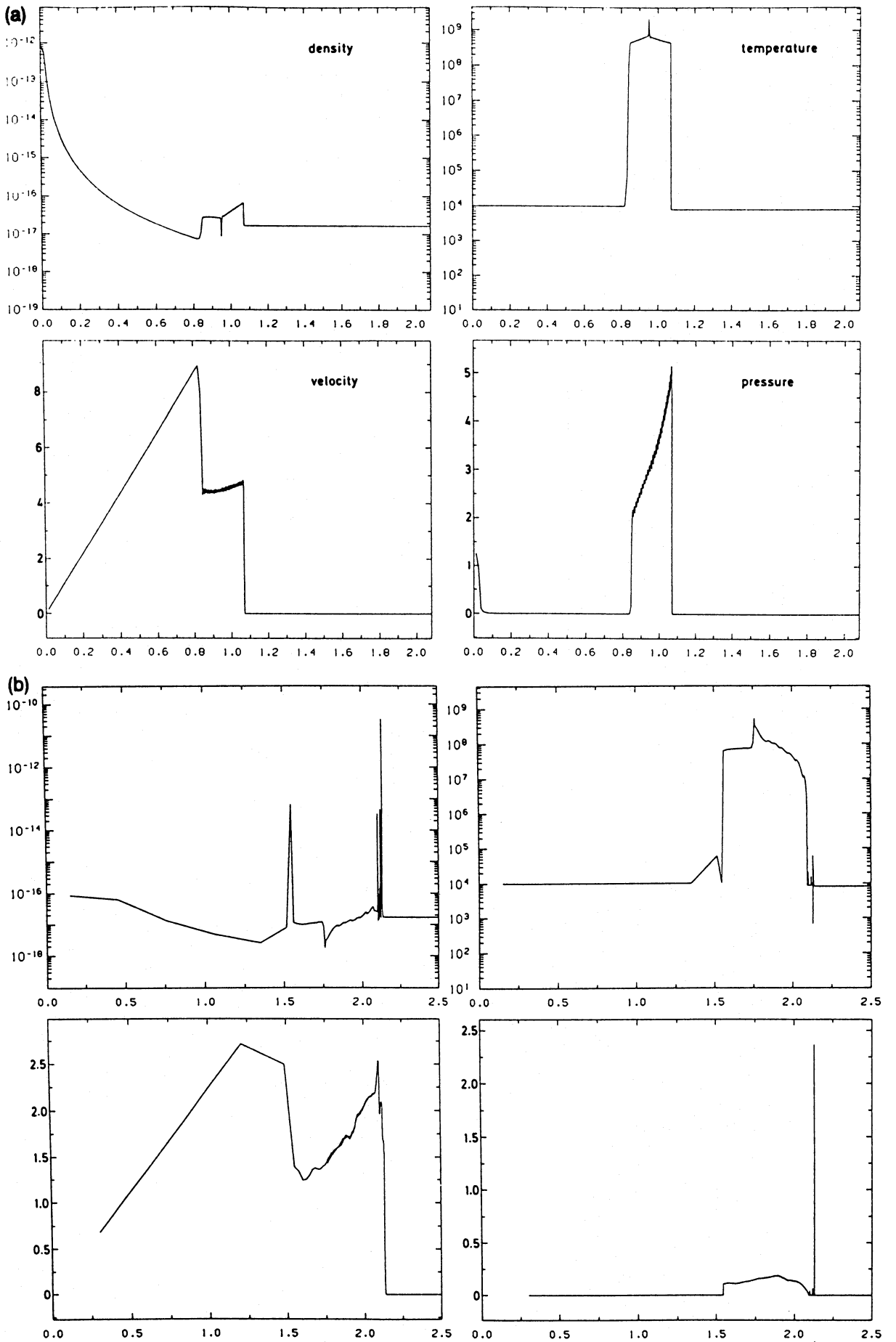

Figure 3. The evolution of remnants in a high-density environment. The run of density (g cm^{-3}), temperature (K), velocity (10^3 km s^{-1}) and pressure (dyn cm^{-2}) as a function of distance to the explosion site in units of 10^{-2} pc. Frames (a) and (b) correspond to times $t_{sn} = 0.53$ and 4.5 yr.

© Royal Astronomical Society • Provided by the NASA Astrophysics Data System

Downloaded from https://academic.oup.com/mnras/article/255/4/713/1310600 by guest on 20 August 2022

1992MNRAS.255..713T

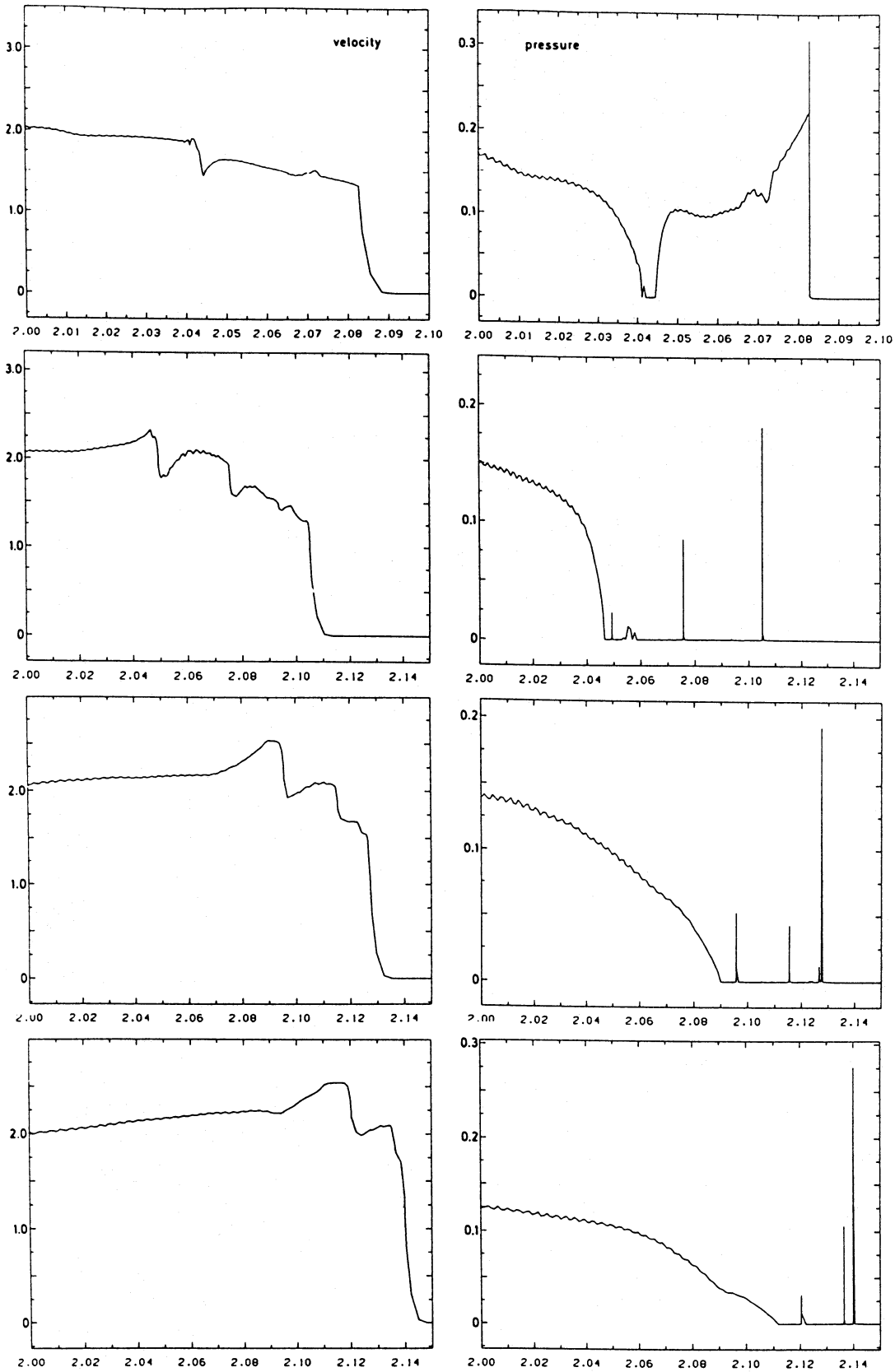

Figure 4. Strong radiative cooling. Details of the flow at the edge of the remnant during thin shell formation. The frames show the run of velocity and pressure at times $t_{sn} = 3.48$, 3.67, 3.89 and 4.0 yr.

Downloaded from https://academic.oup.com/mnras/article/255/4/713/1310600 by guest on 20 August 2022

© Royal Astronomical Society • Provided by the NASA Astrophysics Data System

1992MNRAS.255..713T

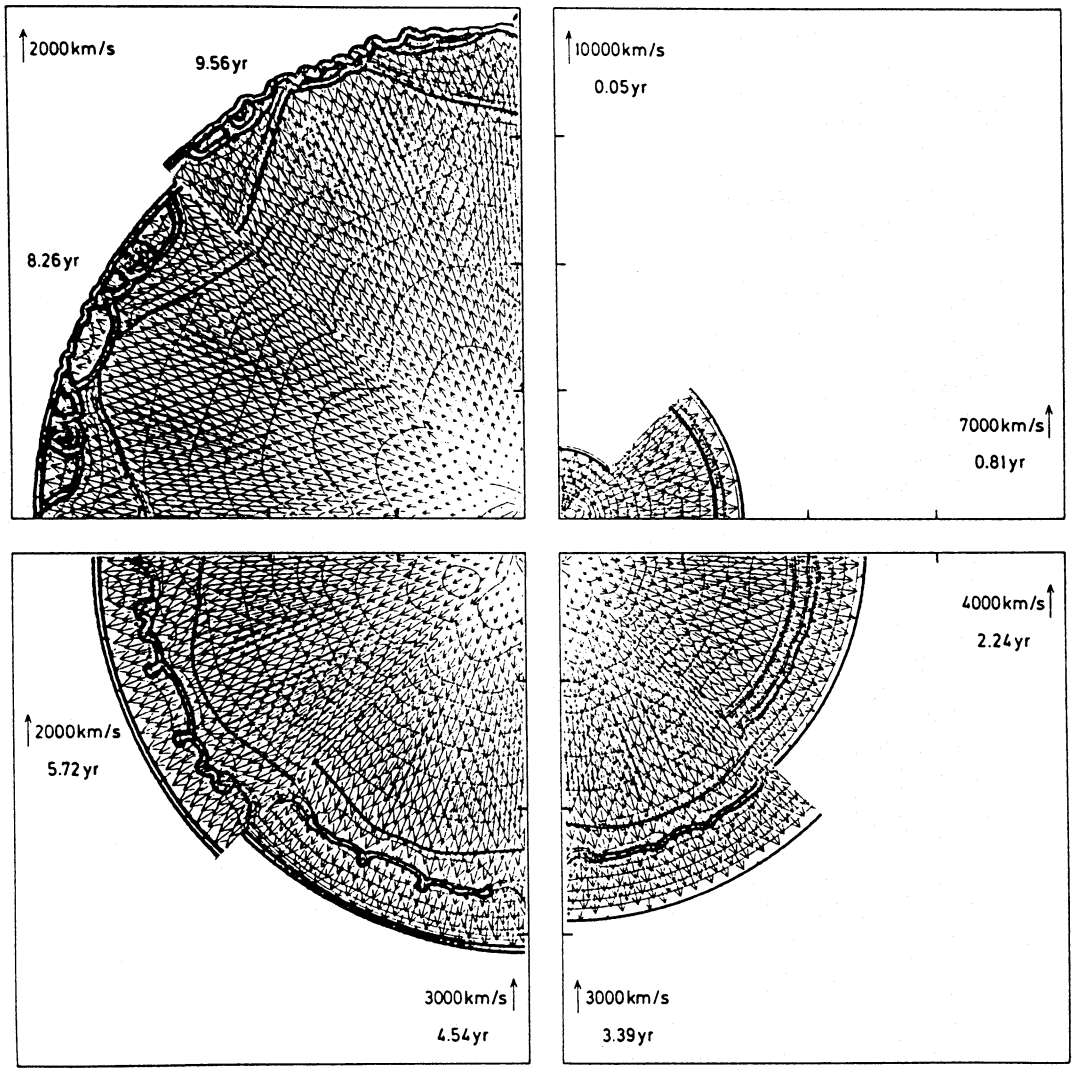

Figure 5. The evolution of supernova remnants in a high-density medium. Two-dimensional representation of the density distribution and velocity field, with scale as indicated at the various times. The contours are logarithmically spaced with $\delta \log (n) = 0.2$. The distance between consecutive tick marks in the frame is 0.02 pc.

Further models with different conditions are under investigation and the details will be discussed in a forthcoming communication.

Finally, it is interesting to compare the time at which the shell formation occurs and the temperature and t_{sg} derived from analytical treatments (e.g. Cox 1972; Falle 1981; Wheeler *et al.* 1980). Fig. 6 shows the results from numerical simulations with $E_0 = 10^{51}$ erg (open circles) and the simple analytical formula for t_{sg} (solid line) discussed by Wheeler *et al.* (1980; see equation 1). The figure also includes a lower bound for the time required for ejecta thermalization, t_{th} (dotted lines). The analytical results can be applied only when $t_{sg} > t_{th}$, and this occurs when $n_0 < 5.0 \times 10^5$ cm^{-3}. For these densities, thin shell formation occurs at about $\sim 2.5\, t_{sg}$. At higher densities, $n_0 > 5.0 \times 10^5$ cm^{-3}, the analytical formula is not valid but, as can be seen from the figure, it still maintains the same relationship with the time of shell formation. This fortunate coincidence can be used to estimate the time of shell formation when numerical simulations are lacking.

2.4 The ionizing spectrum of the cooling region

The temperature structure of the cooling region is, in general, bounded by the isobaric and isochoric cases (Franco *et al.*, in preparation) and, given the small temporal and spatial dimensions of the cooling process, expansion effects can be neglected. The isobaric regime can be approximated by the post-shock pressure (i.e. $nT = 4 n_0 T_s$) and the isochoric regime by the post-shock density (i.e. $n = 4 n_0$). These two cases, maximum compression in the isobaric (constant pressure) regime and no further compression at all in the isochoric (constant density) one, represent the extreme conditions in which cooling may occur. For an optically thin plasma in collisional equilibrium, the cooling function can be written as $\Lambda = \Lambda_0 T^\beta$ and the corresponding cooling rate per gas particle is

$$\dot{\varepsilon} \simeq 2 n_0 T_s \Lambda_0 T^{\beta - 1}, \quad \text{isobaric,} \tag{13}$$

and

$$\dot{\varepsilon} \simeq 2 n_0 \Lambda_0 T^\beta, \quad \text{isochoric,} \tag{14}$$

Downloaded from https://academic.oup.com/mnras/article/255/4/713/1310600 by guest on 20 August 2022

© Royal Astronomical Society • Provided by the NASA Astrophysics Data System

1992MNRAS.255..713T

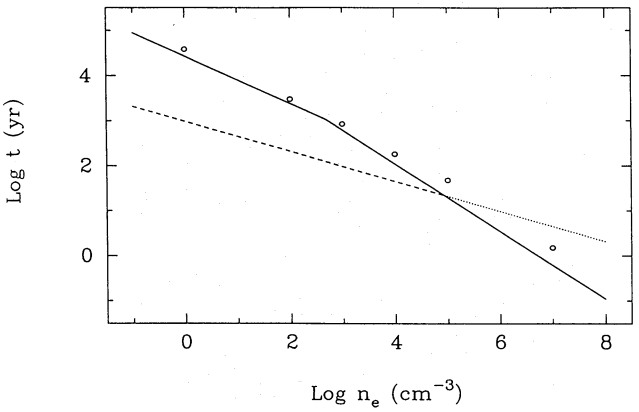

Figure 6. The time-scale for cooling of remnants in a constant density medium. The time at which radiative cooling becomes important, t_{sg}, is plotted for a range of interstellar matter density (n_0). The time t_{sg} presents a change in slope at $n_0 \sim 5\times10^2$ cm^{-3} due to the different cooling rate–temperature dependence of line radiation and free–free cooling, the latter of which becomes the relevant coolant in the large-density cases. Also shown are the values obtained from the numerical calculations, which indicate the onset of radiative cooling before thermalization is completed for values of $n_0 \geq 10^5$ cm^{-3}. The thermalization time t_{th} is defined as the time required by a 10^4 km s^{-1} forward shock to sweep up 100 $M_\odot$. The dashed extension to the t_{th} curve indicates that, if radiative cooling becomes important behind the reverse shock, then the thermalization of the ejected matter is even further delayed due to the weakening and withdrawal of the reverse shock.

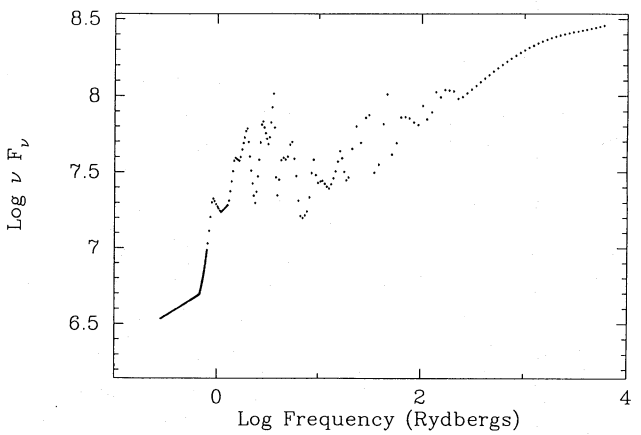

Figure 7. Ionizing spectrum emerging from a radiative shock with post-shock temperature $T_s = 10^8$ K ($v_s \simeq 2.5\times10^3$ km s^{-1}). The flux units are arbitrary.

where the post-shock temperature is $T_s = 3\mu v_s^2/(16k)$, T is the temperature down-stream, and μ is the mass per gas particle (i.e. about 1.4 m_H/2.3 for cosmic abundances). The parameters of the cooling function depend on the plasma temperature: $\beta \simeq -0.5$ (line cooling) with $\Lambda_0 \simeq 10^{-19}$ erg cm^3 s^{-1} K$^{1/2}$ within the range 10^5 K $< T < 3\times10^7$ K, and $\beta = 0.5$ (bremsstrahlung) with $\Lambda_0 \simeq 10^{-27}$ erg cm^3 s^{-1} K$^{-1/2}$ for $T > 3\times10^7$ K (e.g. Raymond *et al.* 1976; Gaets & Salpeter 1983).

The rate of temperature change behind the shock front is $dT/dt \simeq 2\dot{\varepsilon}/(3k)$ and, for a constant flow velocity of $v_s/4$, the corresponding temperature gradients are

$$\frac{dT}{dr} \simeq \frac{8\dot{\varepsilon}}{9kv_s} \simeq \frac{16n_0\Lambda_0}{9kv_s} T_s T^{\beta-1}, \qquad \text{isobaric,} \tag{15}$$

$$\frac{dT}{dr} \simeq \frac{16n_0\Lambda_0}{9kv_s} T^{\beta}, \qquad \text{isochoric,} \tag{16}$$

Once the two extreme temperature gradients are known, one can compute the main features of the photon spectrum emerging from the cooling region. UV line emission from heavy elements dominates the cooling below $T_0 \sim 3\times10^7$ K and we use the line cooling results given by Daltabuit *et al.* (1978). The free–free emission per unit volume and unit frequency is (e.g. Lang 1980)

$$f_\nu \simeq 3.7\times10^{-38} n^2 T^{-1/2} \ln(4.7\times10^{10} T/\nu) \exp(-h\nu/kT)$$

$$\text{erg cm}^{-3}\,\text{s}^{-1}\,\text{Hz}^{-1}, \tag{17}$$

where the Gaunt factor has been approximated by the logarithmic term, and the variables are in cgs units. Thus the spectrum of the outcoming free–free flux is

$$F_\nu \simeq \frac{1}{2}\int_{\Delta R} f_\nu dr = \frac{1}{2}\int_{\Delta T} f_\nu \left(\frac{dT}{dr}\right)^{-1} dT. \tag{18}$$

Using the temperature gradients given in equations (15) and (16), the integrated flux becomes

$$F_\nu \simeq A\int_{\Delta T} T^\gamma \ln(B T/\nu) \exp(C\nu/T)\, dT, \tag{19}$$

where $C = -h/k$, $B = 4.7\times10^{10}$ K^{-1} s^{-1}, A is a constant depending on the temperature range, and the exponent γ takes the values -2, -1, and 0, depending on the case (isobaric or isochoric) and temperature range. This integral has no analytical solutions, but can be easily estimated numerically.

The sum of F_ν for an intermediate case between isobaric and isochoric, and UV line cooling from Daltabuit *et al.* (1978) is given in Fig. 7. The ordinate has arbitrary units. The resulting 'power-law'-like spectrum closely resembles that believed to photoionize the BLR of QSOs. The spectrum is similar for both the main shock moving into the interstellar medium and the reverse shock thermalizing the ejecta. The value of the power-law index depends on the case and temperature range and, for the case illustrated in the figure, is in the neighbourhood of 0.5. The contribution from the Compton tail created within the hot cavity (e.g. Fransson 1982) was also computed, but, given the relatively low column density of the high-temperature gas ($\sim 10^8$ K), its contribution to the ionizing spectrum is negligible.

When cooling instabilities appear, the temperature structure will be oscillating between the isobaric and isochoric cases. Thus both the flux and the spectral form will be correspondingly oscillating from one case to the other. This variability is time-dependent and cannot be analysed with our analytical approach. Note, however, that the variability should have time-scales of the order of t_c and the zone in which it originates has a size of the order of r_c (see equations 11 and 12).

Downloaded from https://academic.oup.com/mnras/article/255/4/713/1310600 by guest on 20 August 2022

© Royal Astronomical Society • Provided by the NASA Astrophysics Data System

1992MNRAS.255..713T

3 PHOTOIONIZATION MODELS

Photoionization models are parametrized by the luminosity and shape of the ionizing continuum, the density, column density and chemical composition of the gas and the ionization parameter. In this section we present the photoionization calculations computed using the program CLOUDY version 76.03 kindly made available by Dr Gary Ferland. A good description of the program is given by Ferland (1990).

To produce a self-consistent model of the BLR, typical values for the density, size, column density, velocity of the cooled regions of gas, and ionizing flux of the two radiative shocks, have been computed from the analytic and numerical hydrodynamical models of the previous sections, to be used as input parameters in the calculations of the ionization structure of the remnants (see Table 1).

3.1 Input parameters

A schematic view of the remnant at $t = t_{sg}$ is presented in Figs 8(a) and (b). The adopted input parameters are listed in Table 1. There are three different sources of ionizing radiation: the two radiative shocks and the hot cavity. Their luminosity, size and temporal behaviour are given by the hydrodynamical models of Section 2. The shape of the spectrum emitted by the cooling material behind the shocks is that computed in Section 2.4. Four cool regions are exposed to the ionizing radiation: the two shells, the unshocked ejecta and the circumstellar material. Their sizes, densities and column densities come from the models.

Half of the luminosity of the outer shock will be emitted outward and thus photoionize the unperturbed circumstellar material. The other half will be emitted inwards and will photoionize the outer shell. A similar situation holds for the reverse shock; half of its luminosity will photoionize the unshocked SN ejecta and the other half will photoionize the inner shell. Both shells are optically thick to the ionizing radiation, so we assumed that no radiation from the outer shock reaches the inner shell and vice versa. Only the hard X-rays are able to cross the cool shells, but their inclusion does not change the results appreciably.

Table 1. Parameters for reverse and leading shock for $n_e = 10^7$ cm^{-3}.

	230days = 1 t_{sg}		920days = 4 t_{sg}	
	RS	LS	RS	LS
V_{shell}(km s^{-1})	6000	4600	2000	1700
log R_{shock}(cm)	16.3	16.5	16.7	16.7
log T_{shock}(K)	7.5	8.5	7.3	7.6
log L_{shock}(erg s^{-1})	42.2	43.2	41.3	42.3
n_{shell}(cm^{-3})	10.0	12.0	9.0	11.3
σ_{shell}(cm^{-2})	23.0	23.0	23.0	23.0
U_{shell}	-2.06	-4.09	-2.74	-4.17
	HIL	LIL	HIL	LIL
log L Hβ(erg s^{-1})	40.46	41.18	39.26	40.72
Lyα/ Hβ	7.1	1.10	32.	3.53
Hα/ Hβ	2.95	2.95	11.9	5.13
Pα/ Hβ	0.26	0.20	1.4	0.30
CIII] / Hβ	2.95	–	9.61	–
CIV / Hβ	18.2	–	4.0	–
MgII / Hβ	9.6	1.9	80.	4.4

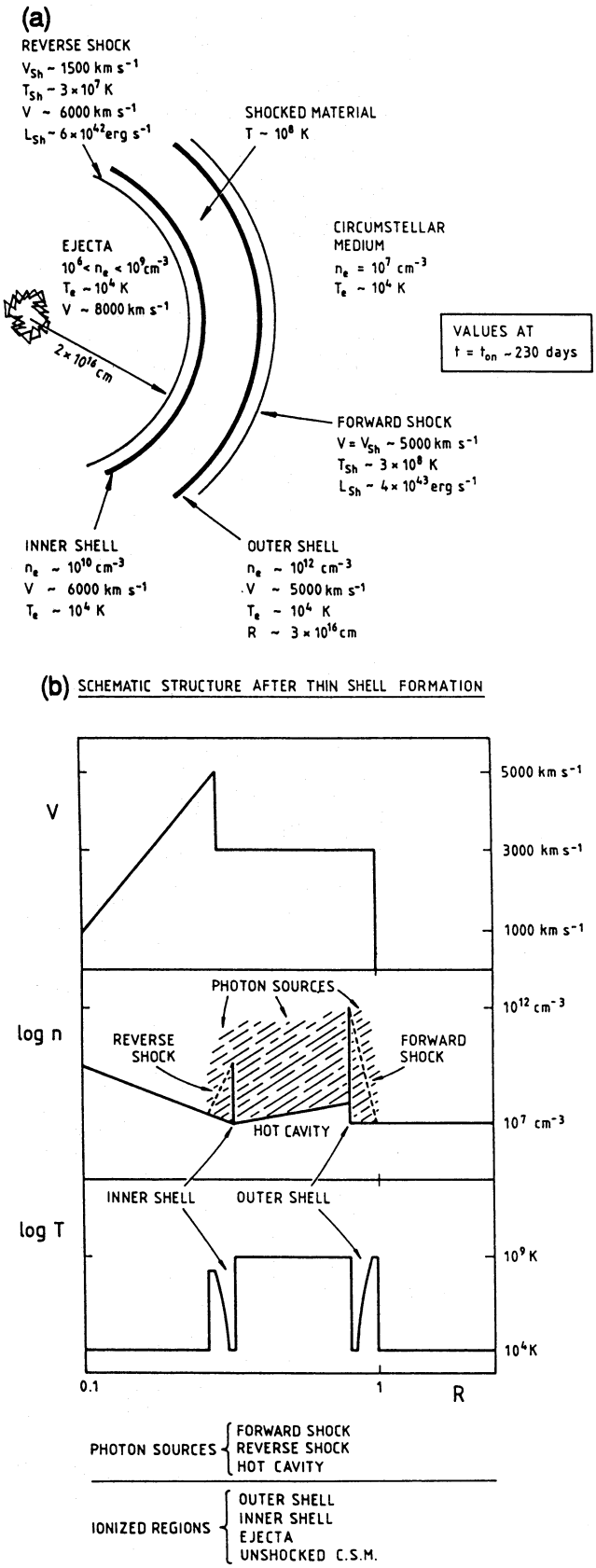

Figure 8. Schematic views of the remnants at $t = t_{sg}$. The parameters are those listed in Table 1. There are three different sources of ionizing radiation: the two radiative shocks and the hot cavity, ionizing four cold regions: the ejecta, both shells and the circumstellar material. Frames (a) and (b) refer to 2D and 1D views.

Downloaded from https://academic.oup.com/mnras/article/255/4/713/1310600 by guest on 20 August 2022

© Royal Astronomical Society • Provided by the NASA Astrophysics Data System

1992MNRAS.255..713T

Given its density and temperature, the hot cavity will emit most of the radiation as free–free in the hard X-ray region; half of it will also contribute to the ionization of the outer shell and the other half will ionize the inner shell. Therefore, apart from the chemical composition, the output parameters of the hydrodynamical models define all the input parameters for the ionization models. In selecting the chemical composition we have to take into account that, while the outer shell is composed mainly of shocked circumstellar material with about solar composition, the inner shell is composed of metal-rich SN ejecta. Our assumed abundances reflect these facts in that we have taken solar composition for the outer shell and circumstellar material, and three times solar for the ejecta and the inner shell.

The dimensionless ionization parameter is

$$U=\frac{\Sigma}{n_e c}$$

where Σ is the rate per unit area of ionizing photons at the surface of the gaseous shell, n_e is the electron density and c is the speed of light. As the emitting shocks are close to the ionized shells, the ionization parameter is completely determined by the hydrodynamical results.

We have computed models for each of the four ionized regions. These are in order of decreasing radius, the unshocked circumstellar material, the outer shell, the inner shell and the unshocked ejecta. Each model is computed independently and the resulting spectrum is the sum of all the four components. In practice, most of the broad-line luminosity comes from the two shells and the ejecta.

Two different epochs were computed, $t=t_{sg}$ and $t=4t_{sg}$. The results for the most intense lines are listed at the bottom of Table 1. A more complete set is listed in Table 2. A quick inspection of Table 1 shows that only low-ionization lines are emitted in the outer shell and that a combination of high-ionization and low-ionization lines comes from the inner shell and, in a smaller proportion, from the ejecta. This behaviour is a consequence of both the relative shock strengths and the shell density achieved after radiative cooling producing a lower ionization parameter at the outer shell.

Table 2. Computed line ratios for the BLR at (a) $t=t_{sg}$ and (b) $t=4t_{sg}$.

(a)

Line	Ejecta	Inner Shell	Outer Shell	Total
Lyα	41.3	7.11	1.11	2.82
Hβ	1.0	1.0	1.0	1.0
Hα	1.83	2.95	2.95	2.93
Pα	0.12	0.26	0.20	0.21
Balmer C	14.6	11.8	34.6	30.6
HeI 5876	0.21	0.09	0.13	0.13
HeII 4686	0.32	0.04	0.01	0.02
HeII 1640	2.85	0.36	0.10	0.20
CII 1335	0.02	0.44	0.03	0.09
CII] 2326	0.23	2.97	0.07	0.53
CIII 977	2.59	1.33	–	0.26
CIII] 1909	11.5	2.95	–	0.68
CIV 1550	33.3	18.2	–	3.50
NIII] 1750	5.75	0.46	–	0.18
NIV] 1486	5.92	0.58	–	0.20
NV 1240	2.21	0.37	–	0.10
OIII] 1663	14.6	2.52	–	0.68
OIV] 1402	6.50	0.68	–	0.23
OVI 1034	76.0	0.22	–	1.48
MgII 2798	0.34	9.61	1.89	3.08
SiIII] 1893	0.71	2.04	–	0.05
SiIV 1397	3.68	1.13	–	0.25
AlIII 1860	0.21	0.25	–	0.04
Total Fe cooling	2.6	35.6	12.1	15.6
log L Hβ(erg s^{-1})	39.54	40.46	41.18	41.26

(b)

Line	Ejecta	Inner Shell	Outer Shell	Total
Lyα	40.3	31.9	3.53	4.82
Hβ	1.0	1.0	1.0	1.0
Hα	4.22	11.9	5.13	5.35
Pα	0.37	1.40	0.30	0.34
Balmer C	6.60	12.2	3.44	3.76
HeI 5876	0.15	0.36	0.07	0.08
HeII 4686	0.20	0.10	0.01	0.02
HeII 1640	1.91	0.91	0.09	0.13
CII 1335	0.03	0.87	0.03	0.06
CII] 2326	1.50	19.5	0.26	0.92
CIII 977	1.41	0.93	–	0.04
CIII] 1909	10.1	9.61	–	0.42
CIV 1550	60.4	4.04	–	0.70
NIII] 1750	0.87	0.76	–	0.03
NIV] 1486	2.58	0.17	–	0.03
NV 1240	4.18	0.05	–	0.04
OIII] 1663	5.46	2.20	–	0.13
OIV] 1402	2.12	0.19	–	0.03
OVI 1034	80.2	0.01	–	0.75
MgII 2798	1.46	80.2	4.42	6.93
SiIII] 1893	0.26	2.59	–	0.09
SiIV 1397	1.70	0.77	–	0.04
AlIII 1860	0.10	0.26	–	0.01
Total Fe cooling	9.6	135.	12.9	17.0
log L Hβ(erg s^{-1})	38.70	39.26	40.71	40.73

4 DISCUSSION

As we have seen in Section 3 the structural parameters for a SNR evolving in a uniform medium of density $n\sim10^7$ cm^{-3} are very similar to those observed or derived for the BLR in low-luminosity AGN. There are other well-established observational facts which are explained by this simple model.

4.1 The observed line ratios and the two systems of broad lines

The difficulties of single-density photoionization models to explain on the one hand the observed low value of Lyα/Hβ, high Hα/Hβ and the strength of Fe II that suggest high densities in the ionized gas and, on the other, the C IV/C III] ratio suggesting relatively lower densities led Kwan & Krolik (1981) and Collin-Souffrin and collaborators (1988, 1990) to split the broad emission lines into two types: the high-ionization lines (HIL), comprising Lyα C III], C IV, He II, N V, O IV, etc., and the low-ionization lines (LIL) that include the Balmer lines, the Balmer continuum, the Fe II lines, etc. The two different type of lines could be understood if they are produced in two different regions. The HIL come from a highly ionized region with relatively low density ($n_e\sim10^9$

Downloaded from https://academic.oup.com/mnras/article/255/4/713/1310600 by guest on 20 August 2022

© Royal Astronomical Society • Provided by the NASA Astrophysics Data System

1992MNRAS.255..713T

cm^{-3}). The upper density limit is imposed by the requirement that the semiforbidden C III] 1909 line should not be collisionally de-excited. The LIL are emitted by a partially ionized medium with much higher density ($n_e > 10^{11}$ cm^{-3}). Models including a density gradient (Rees, Netzer & Ferland 1991) are a variation of this approach.

This division has a natural counterpart in the SNR model, with the outer shell with $n_e = 10^{12}$ cm^{-3} and $\log(U) \sim -4.0$ producing the LIL, and the ejecta and the inner shell with $n_e = 10^{10}$ cm^{-3} and $\log(U) \sim -2.4$ emitting the HIL. The total predicted line ratios are compared with the observations in Fig. 9. The boxes represent the total range of the observations in a sample of AGN compiled by Kwan & Krolik (1981). The horizontal line close to the centre of the box represents the mean value. The computed total broad-line ratios, i.e. including both shells and the ejecta emission, are indicated by the numbers 1 and 4 corresponding to the hydrodynamical models at $t = t_{sg}$ and $t = 4t_{sg}$ respectively. The adopted time interval covers most of the luminosity range of the evolution of the remnant and therefore should represent the observed range of line ratios in AGN. In low-luminosity AGN ($M_V > -20$), where at any time only one SNR causes the emission, the observed line ratios should go from those given by $t = 1$ when the AGN is bright to those represented by $t = 4$ when it is faint. The model for $t = 4t_{sg}$ shows a lower ionization parameter than that of $t = t_{sg}$. As a consequence, at later times in the evolution of the SNR, the HIL are weaker and the Balmer decrement steeper.

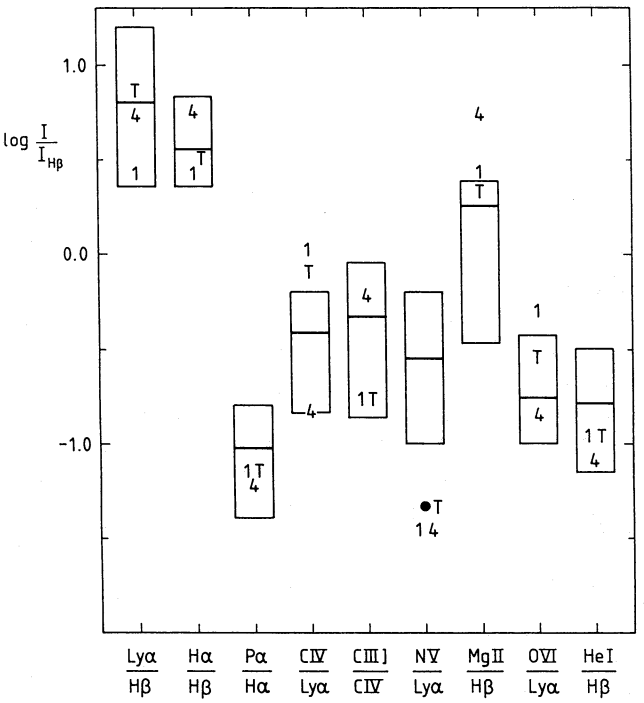

Figure 9. Total predicted line ratios compared with the observations. The boxes represent the total range of the observations in a sample of AGN compiled by Kwan & Krolik (1981). The horizontal line close to the centre of the box represents the mean value. The computed total broad-line ratios, i.e. including both shells and the ejecta emission, are indicated by the numbers 1 and 4 corresponding to the hydrodynamical models at $t = t_{sg}$ and $t = 4t_{sg}$. The adopted time interval covers most of the luminosity range of the evolution of the remnant and therefore should represent the observed range of line ratios in AGN. T_1 and T_4 indicate solutions that also include the narrow emission lines from the dynamically unperturbed interstellar material.

In the case of luminous AGN where the observed spectrum is the sum of several SN and SNRs in different stages of evolution, the observed line ratios should be somewhere between the values obtained for $t = t_{sg}$ and $t = 4t_{sg}$. As we can see from Fig. 9, the computed line ratios are a good match to the observations. All strong line ratios like Lyα/Hβ, Hα/Hβ, C IV/C III], C IV/Lyα, Mg II/Hβ, O VI/Lyα and He I/Hβ, show good agreement with the observations. A noticeable departure is that of N v. Low N v/Lyα is common in many photoionization models of the BLR; the dot in Fig. 9 indicates a typical published value of N v/Lyα (Kwan & Krolik 1981; Rees *et al.* 1991). The observed strong N v in QSOs could be due to an N enhancement in the cores of luminous galaxies. All in all, our model does at least equally well as *canonical* models in predicting the observed line ratios of the BLR.

4.2 The size, variability and luminosity scaling law

The size of the remnant for our adopted density is, at the time it becomes radiative, about 0.02 pc in diameter (or about 23 light-days) and twice that value for $t = 4t_{sg}$. This is the shortest observable time-scale for events involving the whole remnant. The evolution of the remnant results in a secular decay in the luminosity of the shocks, which has an e-folding time larger than both the crossing time and that for cooling instabilities. Radiative instabilities appear in our models after the onset of the radiative phase. The gas cools nearly isobarically from 3×10^8 K to the minimum of the cooling curve at 3×10^7 K, in about one cooling time ($t_{cool} \sim$ 240 d). Afterwards, the cooling time is reduced to $t_{cool} \sim 6$ d. At this moment the cooling instability sets up, and an intense and short burst of mainly extreme UV emission with duration of order of the cooling time is emitted. This occurs independently in both the forward and reverse shocks. The integrated energies for these events are $E \sim 2 \times 10^{49}$ erg and they reach luminosities about $L \sim 4 \times 10^{43}$ erg s^{-1}. Thus an observer will see a sudden increment in the emitted luminosity with duration of about 23 to 50 d and luminosities about $L \sim 4 \times 10^{43}$ erg s^{-1}. These values are very similar to the short-term variations detected in most of the well-sampled low-luminosity Seyfert 1 galaxies (Dibai & Lyutyi 1976; Terlevich & Melnick 1987).

Thus the resultant luminosity output has long-term variations of a few hundred days with energies of about $E \sim 10^{51}$ erg and, on average, luminosity $L \sim 3 \times 10^{43}$ erg s^{-1} with a superposed population of flares with duration between 20 and 50 d with energies $E \sim 2 \times 10^{49}$ erg and average luminosity $L \sim 4 \times 10^{43}$ erg s^{-1}. The flares have a much softer spectrum than the long-term component.

One of the central problems in the understanding of the BLR of AGN is related to the fact that for a large range of total luminosity, from low-luminosity Seyferts to luminous QSOs, the emitted emission line spectrum looks roughly the same. At the same time, it is possible to reproduce this spectrum only with a very restricted range of the ionization parameter. Thus, in the canonical scenario the intrinsic parameters of the BLR should scale with luminosity to give what is basically the same emission line ratios and line

Downloaded from https://academic.oup.com/mnras/article/255/4/713/1310600 by guest on 20 August 2022

© Royal Astronomical Society • Provided by the NASA Astrophysics Data System

1992MNRAS.255..713T

widths independently of the luminosity of the central object (but see Joly *et al.* 1985). In the starburst scenario, high-luminosity objects have a collection of SNRs at any given time within the star-forming region, and therefore no *direct* change in the spectral properties with luminosity is expected.

Variability studies of large samples of AGN (Pica & Smith 1983; Cristiani, Vio & Adreani 1990; Hook *et al.* 1991) show that luminous QSOs are less variable than low-luminosity Seyferts. The analysis of the best data sets of photometry of QSOs over a long time is consistent, if not suggestive, of the variability originating in SN-size events (Terlevich 1990b).

A more detailed discussion of variability will be given in a forthcoming communication.

4.3 The absence of broad forbidden lines

An interesting aspect of the SNR model is that it gives a natural explanation for the lack of broad forbidden lines in AGN. To avoid collisional de-excitation of the most intense forbidden lines, the densities should be lower than $n_e \sim 10^6$ cm^{-3}. The equations of Section 2.1 indicate that, for shell densities below 10^6 cm^{-3}, shock and shell velocities will be below 500 km s^{-1} at $t > t_{sg}$. Therefore no broad forbidden lines will be produced in the outer shell in such a case. The numerical models indicate that this is also true for the reverse shock and the inner shell.

4.4 The stability of the BLR gas

The survival of the high-density gas responsible for the broad emission lines in the BLR is an outstanding problem in the 'canonical scenario'. The possibility of a hot medium in pressure equilibrium with the high-density clouds is not supported by the measurements of X-ray column densities in Seyfert nuclei and, as pointed out by Perry & Dyson (1985), at least for luminous AGN the confining medium should be Compton thick. Possible alternatives are stellar atmospheres (Edwards 1980), transient clouds from SN shocks (Perry & Dyson 1985) or magnetic confinement (Rees 1987).

The SNR model on the other hand does not have such a problem. The emitting regions are stable for all the relevant evolutionary times, and replenished by new SNR produced by stellar evolution in the young cluster.

4.5 The X-ray column density

Most of the observed X-ray emission in our model corresponds to the outward emission of the forward shock. This radiation has to ionize the unshocked circumstellar material before leaving the remnant, and thus the observed X-ray column density refers only to the circumstellar material in front of the forward shock. Our photoionization models indicate that, for a reasonable range of total mass ejected during the pre-SN stage, the circumstellar material is always highly ionized by the luminosity of the forward shock. For a range of outer radius from 5×10^{16} to 10^{17} cm, the column density of H I is about 10^{16} to 10^{18} cm^{-2}, in agreement with the observations (Turner & Pounds 1989). As the remnant evolves, the shock becomes weaker and moves closer to the edge of the circumstellar matter, so both the ionization fraction and the column density decrease, leading to a roughly constant total X-ray column density.

4.6 Balmer line profile ratios

Since shock and incoming ejecta velocities diminish with time, old remnants will have narrower lines than young ones. In luminous AGN therefore, where the line emission is the sum over several remnants, the line wings will be preferentially emitted by young remnants while the cores of the lines will come from the older ones. Hence model 1 is indicative of the relative line intensities for the wings of the lines, while model 4 gives the intensities corresponding to the cores of the lines. As the shock velocity decreases from ~ 5000 km s^{-1} at $t = t_{sg}$ to ~ 1500 km s^{-1} at $t = 4t_{sg}$, the Hβ/Hα ratio decreases from ~ 0.35 to ~ 0.17. This relationship is very similar to that observed by Crenshaw (1986) between the Balmer decrement and the velocity shift from the line core. He found that, in most of the AGN observed, the Hβ/Hα ratio decreased from about 0.35 at 4000 km s^{-1} to about 0.2 at the core.

4.7 Emission line shifts

The bulk of HIL intensity originates in the inner shell and the unshocked ejecta, where the observer sees the largest ionized gas velocities. Thus an important prediction of our model is that the HIL will, on average, be broader than the LIL. In addition, since, due to the geometry, the opacity of the SN ejecta affects the HIL more than the LIL, a large blue asymmetry is expected in the HIL, in particular during the brightest early phases of the evolution. This difference should be apparent as a relative blueshift of the HIL with respect to the LIL. This type of behaviour has been reported by Espey & collaborators (Espey *et al.* 1989). Blueshifts of up to 1500 km s^{-1} were found between the Lyα, C III] and C IV lines and Hα.

4.8 The X-ray spectrum emitted by a population of SNR

The X-ray spectrum of the starburst will be the sum of the contributions from all SNR. It is interesting to estimate the shape of the resulting spectrum. Remnants evolving in the high-density environment will have shock temperatures well in excess of 10^7 K and emit most of the luminosity in X-rays. At these temperatures, the main cooling mechanism is free–free emission, as described in Section 2.4, and the spectrum can be approximated by a power law, say ν^{-x}, with x in the range ~ 0.2 to ~ 0.5, according to the case and temperature range. The time evolution of this spectrum also depends on the location of the frequency at which the emission peaks, ν_m. Thus the time evolution can be written as

$$f_\nu \propto f_{\nu_m}(t)\, \nu^{-x} \quad \text{for } \nu < \nu_m$$

$$f_\nu = 0 \quad \text{for } \nu > \nu_m,$$

where $f_{\nu_m}(t)$ is the time dependence of the SNR luminosity at the frequency ν_m. Given that ν_m is proportional to the shock temperature, the decrease in ν_m can be written as the usual decrease of post-shock temperature with time, $\nu_m \propto T_{sh} \propto t^{-\beta}$, where the exponent β is positive. Also, the luminosity of the SNR, L_{SNR}, is proportional to the shock luminosity, and the

Downloaded from https://academic.oup.com/mnras/article/255/4/713/1310600 by guest on 20 August 2022

© Royal Astronomical Society • Provided by the NASA Astrophysics Data System

1992MNRAS.255..713T

time evolution can be written as $L_{SNR} \propto L_{sh} \propto t^{-\gamma}$, where γ is also positive. Note that the values of β and γ can be derived from a simple dimensional analysis for a wide variety of shock conditions. The spectrum peaks at $\nu \sim \nu_m$, and the luminosity is proportional to $L_{sh} \propto \nu_m f_{\nu_m}$, so $f_{\nu_m}(t) \propto (L_{sh}/\nu_m) \propto t^{(\beta-\gamma)}$, and the integrated flux of an ensemble of remnants with different ages can be written as

$$F_\nu \propto \int f_\nu dt \propto \int \nu^{-x} t^{(\beta-\gamma)}\, dt \propto \nu^{-x-(\beta-\gamma+1)/\beta}.$$

The sum over a population of remnants, with a uniform distribution of ages and each emitting thermal free–free, therefore also produces a power-law spectrum for X-rays.

It is interesting to estimate the slope of the power law for different conditions in the remnant evolution. For the pressure-modified snow-plough solution (see Section 3), $\gamma = \frac{11}{7}$, and $\beta = \frac{10}{7}$, whereas $\gamma = \frac{7}{4}$, and $\beta = \frac{3}{2}$ for momentum conservation. Thus, for these different cases, the value remains roughly constant with

$$\frac{\beta - \gamma + 1}{\beta} \sim 0.6; 0.5.$$

The power law would extend from an upper limit of about 40 keV (when young remnants are present) down to about 1 keV. Below 1 keV the contribution by line cooling from different remnants dominates the emitted spectrum and produces a bump on the power law.

This spectral shape is very similar to that observed in AGN. Recent X-ray observations have shown a 2–10 keV power-law slope in the range -0.5 to -1.0 with a mean index of about -0.8. A soft excess above the simple power-law fit is found in many AGN (Wilkes & Elvis 1987; Turner & Pounds 1989). At 0.2 keV this excess is as large as the power-law extrapolation.

4.9 The NLR line ratios

Most of the outward emission of the leading shock leaves the circumstellar shell and ionizes the low-density interstellar medium. For densities $n_e \sim 100$ cm^{-3}, the size of the ionized region around a young remnant is about 100 pc. As the light crossing time of this region is larger than the lifetime of the remnant, the interstellar medium must be ionized by the time-averaged spectrum of the whole SNR population. We therefore calculated the emission line ratios of the ionized interstellar medium, using the average ionizing radiation of the ensemble of remnants computed in Section 4.8. As can be seen from the results in Table 3, the line ratios observed in the NLR of AGN are readily explained by photoionization of a low-density interstellar medium of solar composition by the ensemble of SNRs.

Addition of the NLR emission to the computed BLR ratios introduces some small changes in the predicted values. This is shown in Fig. 5, where T indicates the predicted total line ratios at $t = t_{sg}$. The total values include the broad-line fluxes for $t = t_{sg}$ plus the emission from the dynamically unperturbed interstellar material. So the distance between 1 and T gives an estimate of the relative importance of the BLR and NLR in each line ratio.

Table 3. Computed line ratios for the NLR.

Line	Intensity
OVI 1034	4.60
Lyα	24.9
NV 1240	1.05
SiIV 1397	0.05
OIV] 1402	0.61
NIV] 1486	0.49
CIV 1550	17.4
HeII 1640	1.72
OIII] 1663	0.56
NIII] 1750	0.11
SiIII] 1893	0.15
CIII] 1909	2.58
CII] 2326	0.25
MgII 2798	1.14
[NeV] 3426	1.13
[OII] 3727	1.84
[NeIII] 3869	1.40
[SII] 4072	0.04
[OIII] 4363	0.26
HeII 4686	0.18
Hβ	1.00
[OIII] 5007	22.3
[NI] 5200	0.09
[FeXIV] 5303	0.04
HeI 5876	0.10
[FeVII] 6087	0.10
[OI] 6300	0.60
[NII] 6548	0.31
Hα	2.75
[NII] 6584	0.93
[SII] 6716	0.73
[SII] 6731	0.52
[ArIII] 7136	0.10
[OII] 7325	0.03
Pα	0.15
Total Fe cooling	2.00
Balmer C	4.22
log L Hβ(erg s^{-1})	40.70

5 CONCLUSIONS

The calculations and comparison with observations presented here indicate that BLR models involving young luminous SNRs can explain a large number of the observed properties of the BLR of AGN with a minimum number of free parameters.

The computed line intensity ratios are in excellent agreement with those observed in the BLR, and the model output displays the following additional features:

bolometric luminosity of more than 10^{43} erg s^{-1};
emission line width of about 5000 km s^{-1};
size of about 0.01 pc;
two main broad-line emitting regions, one with high density ($n_e \sim 10^{12}$ cm^{-3}) and low ionization (LIL), and the other of lower density ($n_e \sim 10^{10}$ cm^{-3}) and higher ionization (HIL);
column density of ionized gas of about 10^{23} cm^{-2};
total mass of ionized gas in the BLR from about 1 $M_\odot$ to about 10 $M_\odot$;

Downloaded from https://academic.oup.com/mnras/article/255/4/713/1310600 by guest on 20 August 2022

© Royal Astronomical Society • Provided by the NASA Astrophysics Data System

1992MNRAS.255..713T

power-law ionizing spectrum of the form $f_\nu \propto \nu^{-0.5}$ up to ~ 100 keV with a UV bump between 10 and 400 eV;
absence of broad forbidden lines;
stable BLR emitting gas;
rapid UV and broad-line variability with time-scale of about 10 days;
long-term X-ray and broad-line variability with time-scales from weeks to months;
small X-ray absorption column density; and
redshift and line-width differences between HIL and LIL systems.

On balance it is remarkable that the simple SNR model can successfully explain the observed values of so many parameters of the BLR with basically only one free parameter and without resorting to any fine tuning. This in turn suggests that fast radiative shocks are a very reasonable model for the BLR, independent of the source of energy.

If our hypothesis is correct, it should be possible to extend this simple model to explain the observed variability of Seyfert nuclei in the optical and UV spectral range. A detailed discussion of the variability caused by strong radiative cooling behind the remnant shocks will be given in forthcoming communications.

Our initial conditions are adequate for a low-mass SN progenitor that represents the most common event. More massive progenitors will have somewhat different evolution perhaps involving slower shocks and more massive circumstellar shells. In the near future, much knowledge will be gained by the detailed comparison of theoretical predictions of the model with the observed evolution of 'Seyfert-like' SNRs.

Future work will also explore the origin of the rapid X-ray variability and the details of the X-ray spectrum of AGN.

ACKNOWLEDGMENTS

We thank Bob Carswell, Angeles Díaz and Elena Terlevich for discussions and suggestions to improve this paper, and Andy Fabian, Gary Ferland, Martin Rees and Andy Robinson for discussions. We also thank Gary Ferland for making available to us his photoionization code. The hospitality of the RGO, IAC and ESO are gratefully acknowledged.

REFERENCES

Avedisova, V. S., 1974. *Soviet Astr.*, **18,** 283.
Band, D. L. & Liang, E. P., 1989. *Astrophys. J.*, **344,** 366.
Bertschinger, E., 1986. *Astrophys. J.*, **304,** 154.
Chevalier, R. A., 1974. *Astrophys. J.*, **188,** 501.
Chevalier, R. A. & Imamura, J. N., 1982. *Astrophys. J.*, **261,** 543.
Chevalier, R. A. & Liang, J., 1989. *Astrophys. J.*, **344,** 332.
Cioffi, D. F., McKee, C. F. & Bertschinger, E., 1988. *Astrophys. J.*, **334,** 252.
Collin-Souffrin, S., 1990. In: *New Windows to the Universe,* p. 235, eds Sanchez, F. & Vazquez, M., Cambridge University Press, Cambridge, UK.
Collin-Souffrin, S. & Lasota, J.-P., 1988. *Publs astr. Soc. Pacif.*, **100,** 1041.
Cox, D. P., 1972. *Astrophys. J.*, **178,** 159.
Crenshaw, D. M., 1986. *Astrophys. J. Suppl.*, **62,** 821.
Cristiani, S., Vio, R. & Andreani, P., 1990. *Astr. J.*, **100,** 56.
Daltabuit, E., MacAlpine, G. M. & Cox, D. P., 1978. *Astrophys. J.*, **219,** 372.
Díaz, A., Pagel, B. E. J. & Wilson, I., 1985. In: *Active Galactic Nuclei,* p. 171, ed. Dyson, J. E., Manchester University Press, Manchester.
Dibai, E. A. & Lyutyi, V. M., 1976. *Soviet astr. Lett.*, **2,** 90.
Dupree, A. K., 1986. *Ann. Rev. Astr. Astrophys.*, **24,** 377.
Edwards, A. C., 1980. *Publs astr. Soc. Pacif.*, **94,** 634.
Epsey, B. R., Carswell, R. F., Bailey, J. A., Smith, M. G. & Ward, M. J., 1989. *Astrophys. J.*, **324,** 666.
Falle, S. A. E. G., 1975. *Mon. Not. R. astr. Soc.*, **172,** 55.
Falle, S. A. E. G., 1981. *Mon. Not. R. astr. Soc.*, **195,** 1011.
Ferland, G., 1990. *Internal Report (90-02),* Ohio State University Astronomy Department.
Field, G. B., 1964. *Astrophys. J.*, **140,** 1434.
Filippenko, A., 1989. *Astr. J.*, **97,** 726.
Franco, J., Tenorio-Tagle, G., Bodenheimer, P. & Różyczka, M., 1991. *Publs astr. Soc. Pacif.*, **103,** 803.
Fransson, C., 1982. *Astr. Astrophys.*, **111,** 140.
Gaets, T. J. & Salpeter, E. E., 1983. *Astrophys. J. Suppl.*, **52,** 155.
Gull, S. F., 1973. *Mon. Not. R. astr. Soc.*, **161,** 47.
Hook, I. M., McMahon, R. G., Boyle, B. J. & Irwin, M. J., 1991. Preprint.
Imamura, J. N., 1985. *Astrophys. J.*, **296,** 128.
Joly, M., Collin-Souffrin, S., Masnou, J. L. & Notale, L., 1985. *Astr. Astrophys.*, **152,** 282.
Kwan, J. & Krolik, J. H., 1981. *Astrophys. J.*, **250,** 478.
Lang, K. R., 1980. *Astrophysical Formulae,* Springer-Verlag, Berlin.
McCray, R., Stein, R. F. & Kafatos, M., 1975. *Astrophys. J.*, **196,** 565.
McCrea, W. H., 1976. In: *The Galaxy and the Local Group,* eds Dickens, R. J. & Perry, J. E., RGO Bull. 182.
Pagel, B. E. J. & Edmunds, M., 1981. *Ann. Rev. Astr. Astrophys.*, **19,** 77.
Perry, J. J. & Dyson, J. E., 1985. *Mon. Not. R. astr. Soc.*, **213,** 665.
Pica, A. J. & Smith, A. G., 1983. *Astrophys. J.*, **272,** 11.
Raymond, J., Cox, D. P. & Smith, B. W., 1976. *Astrophys. J.*, **204,** 290.
Rees, M. J., 1977. *Q. J. R. astr. Soc.*, **18,** 429.
Rees, M. J., 1978. *Observatory,* **98,** 210.
Rees, M. J., 1984. *Ann. Rev. Astr. Astrophys.*, **22,** 471.
Rees, M. J., 1987. *Mon. Not. R. astr. Soc.*, **228,** 47P.
Rees, M. J., Netzer, H. & Ferland, G. J., 1991. *Astrophys. J.*, **347,** 640.
Różyczka, M., 1985. *Astr. Astrophys.*, **163,** 59.
Shklovskii, I. S., 1960. *Sov. Astr.*, **4,** 885.
Shull, J. M., 1980. *Astrophys. J.*, **237,** 769.
Tenorio-Tagle, G., Bodenheimer, P., Franco, J. & Różyczka, M., 1990. *Mon. Not. R. astr. Soc.*, **244,** 563.
Tenorio-Tagle, G., Różyczka, M., Franco, J. & Bodenheimer, P., 1991. *Mon. Not. R. astr. Soc.*, **251,** 318.
Terlevich, R., 1989. In: *Evolutionary Phenomena in Galaxies,* p. 149, eds Beckman, J. E. & Pagel, B. E. J., Cambridge University Press, Cambridge, UK.
Terlevich, R., 1990a. In: *Windows on Galaxies,* p. 87, eds Fabbiano, G., Gallagher, J. & Renzini, A., Kluwer, Dordrecht.
Terlevich, R., 1990b. In: *Structure and Dynamics of the Interstellar Medium,* p. 343, eds Tenorio-Tagle, G., Moles, M. & Melnick, J., Springer-Verlag, Berlin.
Terlevich, R., 1992. In: *Relationships Between Active Galactic Nuclei and Starburst Galaxies,* eds Filippenko, A. & Lo, K. Y., Astr. Soc. Pacif. Conf. Proc., in press.
Terlevich, R. & Melnick, J., 1985. *Mon. Not. R. astr. Soc.*, **213,** 841 (TM85).
Terlevich, R. & Melnick, J., 1987. In: *Starburst and Galaxy Evolution,* p. 393, eds Thuan, T. D., Montmerle, T. & Tran Than Van, J., Editions Frontiéres, Gif-sur-Yvette.

Downloaded from https://academic.oup.com/mnras/article/255/4/713/1310600 by guest on 20 August 2022

© Royal Astronomical Society • Provided by the NASA Astrophysics Data System

1992MNRAS.255..713T

Terlevich, R. & Melnick, J., 1988. *Nature,* **333,** 239.
Terlevich, R., Melnick, J. & Moles, M., 1987. In: *Observational Evidence for Activity in Galaxies,* p. 499, eds Khachikyan, E. Ye., Fricke, K. J. & Melnick, J., Reidel, Dordrecht.
Turner, T. J. & Pounds, K., 1989. *Mon. Not. R. astr. Soc.,* **240,** 833.
Wheeler, J. C., Mazurek, T. J. & Sivaramakrishnan, A., 1980. *Astrophys. J.,* **237,** 781.
Wilkes, B. & Elvis, M., 1987. *Astrophys. J.,* **323,** 243.
Woosley, S. E., Pinto, P. A. & Ensman, L., 1988. *Astrophys. J.,* **324,** 466.
Woosley, S. E., Weaver, T. A. & Taam, R. E., 1980. In: *Type I Supernovae,* p. 96, ed. Wheeler, J. C., University of Texas, Austin.

Downloaded from https://academic.oup.com/mnras/article/255/4/713/1310600 by guest on 20 August 2022

© Royal Astronomical Society • Provided by the NASA Astrophysics Data System